Local bridging effect of fractured laminated glass with EVA based hybrid interlayers under weathering actions

Jian Yang[a,b,c], Yige Wang[a,b], Xing-er Wang[a,b,d*], Xiaonan Hou[d], Chenjun Zhao[a,b], Jianqiao Ye[d]

[a] State Key Laboratory of Ocean Engineering, Shanghai Jiao Tong University, Shanghai 200240, PR China

[b] Shanghai Key Laboratory for Digital Maintenance of Buildings and Infrastructure, School of Naval Architecture, Ocean and Civil Engineering, Shanghai Jiao Tong University, Shanghai 200240, PR China

[c] School of Civil Engineering, University of Birmingham, Birmingham B15 2TT, UK

[d] Department of Engineering, Lancaster University, Lancaster, LA1 4YW, UK

Abstract: Local bridging ability between fragments including bridging force and adhesion concerns the post-fracture performance of laminated glass (LG). Weathering actions such as heat and lighting radiation can greatly damage bridging ability. The bridging behaviour of fractured LG under diverse weathering actions was examined in this work. Material specimens made of single EVA interlayer and hybrid EVA/PC interlayer, which were developed to provide better degradation resistance and long-term post-fracture performance for LG products, were manufactured. Uniaxial tensile tests on the interlayer specimens and through-crack tensile (TCT) tests on fractured LG specimens were performed after the specimens were exposed to the weathering actions including different temperatures, damp heat, and radiations from laboratory light source. Experimental observations, testing data such as bridging force-displacement relationship, normalized force and stress were analysed to discuss the effects of the weathering actions. Finally, the equivalent adhesion energy was determined to describe the failure of interfacial bridging. It is found that temperature rise to over 60℃ will greatly damage the bridging ability even for the specimens with hybrid interlayers, which also present limited bridging effects when temperature increases to nearly 100℃. Damp heat and lighting treatment are found to have limited effects on the adhesion resistance of hybrid interlayer, although the former may facilitate interlayer rupture and the latter may result in greater degradation of adhesion energy.

Keywords: Laminated glass; Delamination; Weathering action; Ethylene-vinyl acetate; Adhesion

1. Introduction

Transparent laminates such as laminated glass (LG) has been widely adopted in the automotive engineering and construction sector. LG products are vulnerable to dynamic load [1], such as the pedestrian impact in a car accident, blast load [2] or windborne debris hit on the glass structures [3, 4]. The post-fracture capability of LG products [5, 6] is worthy of investigation and a rising trend of corresponding reports can be found in recent years.

Once the glass layers are fractured, three key aspects contribute to the post-fracture performance of LG: (1) the residual resistance of fractured glass by holding fragments together via adhesion to the interlayer; (2) the short term and long term property of interlayer, the former is related to the rupture resistance whilst the latter concerns the safety before replacement of fractured product; (3) the adhesion property of interlayer-glass interface which has significant influence on the post-fracture stiffness and the progressive failure.

The contribution of fractured glass to the post-fracture capability has been extensively studied. Most related works were conducted using experimental [7, 8] and theoretical approaches [9, 10]. The tension stiffening (TS) effect by adhesion to glass fragments, which can contribute to the post-fracture performance through the shear stress transmission between the fractured and intact glass layer, was originally described in Galuppi's work [11]. Biolzi et al. [7] also identified the corresponding stiffening effect due to delamination ratios on the stiffness of ionoplast polymer. Zhao et al. [12] experimentally examined the out-of-plane resistance of fractured LG panels. It is found that greater post-fracture performance can be provided if glass thermal treatment allows for generating larger fragment size. Their work also identifies the positive interlocking effect by holding glass fragments together via alternatively adhesion and interaction. Numerical attempts using combined Voronoi tessellation and finite-discrete element method were also carried out by Wang et al. to investigate the influence of fracture pattern on the stiffness and resistance of fractured tempered glass laminates [13] and beam [14]. The findings so far reveal that the residual resistance of fractured glass is also highly related to the interlayer and adhesion properties [15]. For example, a stiffer interlayer or higher adhesion level will limit the volume expansion of tempered glass fragments at breakage point and hence facilitate integrity of glass layer. Moreover, higher adhesion level can reduce local delamination at the edges of glass fragments and hence retain relatively higher

stiffness of fractured glass laminates.

The interlayer in LG products commonly adopts the same material such as Polyvinyl butyral (PVB), ionoplast polymer (e.g. SentryGlas, SG) or Ethylene Vinyl Acetate (EVA) [16, 17]. Many studies concerning the tensile property of popular interlayers can be found, where key influencing factors such as the time, temperature and strain rate dependency were considered [18-21]. Chen et al. [22] experimentally tested the uniaxial tensile property of ionoplast interlayer, which was popular in the products for load bearing glass structures, at different strain rates and temperatures. Two intervals of strain rate, 10^{-3} s^{-1} to 10^{-1} s^{-1} and 1 s^{-1} to 800 s^{-1}, as well as a temperature range from -40 °C to 80 °C were studied. The results show that higher strain rate and lower temperature result in greater strength and stiffness with a decline in ductility. Xavier [23] conducted a comprehensive experimental study on the tensile behaviour of seven different polymeric films including PVB, SG, EVA and thermoplastic polyurethane (TPU) exposed to thermal cycles, moisture and high temperature. The results show that EVA based interlayers are less affected by the aging factors whilst SG interlayer has the highest stiffness and tensile strength. Dynamical-Mechanical-Thermal-Analysis (DMA) method was also used by Schuster et al. [24] to investigate the thermorheologically complex material behaviour of EVA interlayer. In the post-fracture stage, in particular, if all glass layers are fractured, the interlayers using the same material will lead to unrecoverable deformation of LG due to its relaxation feature and the weight of glass fragments. Other transparent plastics such as acrylic glass (PMMA), polycarbonate (PC) and polyethylene terephthalate (PET) can be laminated with traditional interlayer to promote the long-term load bearing capacity of LG products [25]. Two additional thin PC films (0.20 mm) were found to significantly reduce the long term deformation of fractured triple layered LG beam using two 1.52 mm DG41 PVB interlayers [8]. However, reports concerning hybrid interlayers commonly focused on its enhancement in anti-penetration performance [26], e.g. under bullet hit, while studies on their strength in facilitating the post-fracture behaviour are extremely limited.

Tempered glass will present a trend of volume expansion which is restrained by the adhesion to interlayer at breakage point. The restraint of rapidly dynamic expansion will generate partial delamination at the edges of fragments. A greater partial delamination ratio will result in an evident reduction in the stiffness of fractured glass laminates [9]. Higher adhesion level can reduce the partial delamination and hence retain high post-fracture stiffness. Its delamination can also absorb

more kinetic energy in a dynamic load case. A classic experimental method to examine the adhesion property in the post-fracture stage is the through-crack tensile (TCT) test [27]. TCT specimen is devised to simulate the local bridging behaviour between glass fragments connected by interlayer [28]. Fourton et al. [29] adopted TCT test method to examine the coupling between adhesion, delamination and energy dissipation in PVB LG. The effects of loading rate, interlayer thickness and surface treatment were investigated. It is found that although higher adhesion level increases the energy used to propagate the delamination, the energy dissipated in the stretching of PVB volume is not affected. Samieian et al. [30] also adopted TCT test method to study the adhesion of PVB LG in a temperature range of 20 °C to 60 °C. It is observed that the adhesion at constant temperature is load rate dependent whereas that is temperature independent at a constant load rate. It is also worth noting that as two pre-cracks are in the middle of glass layers, there are not facing stress fronts in TCT tests, hence, the merging of the stress diffusion zones will lead to the absence of TS effect [11]. To overcome this shortcoming, offset-crack tension (OCT) test [31] was used to model a more realistic mechanism of LG although it might not be suitable to identify the adhesion energy. Other test methods such as compression shear test (CST) [32, 33] and pummel test [34] were also used to test the adhesion level. A commonly adopted design of CST test inserts LG specimen in the interface plane of two metallic units inclined of 45°, which can guarantee that the compression and the shear components have the same intensity [35]. The latter test classifies the adhesion level using different pummel values, which strongly depends on the experience of the researcher who conducts the test. It is well known that both the adhesives and adhesive interfaces are highly sensitive to weathering actions. For example, PVB material and its adhesion to glass were found to have significant strength degradation and even delamination under moisture [23, 36]. Delamination of other composites using glass, plastic and polymeric interlayer in service condition was also reported, in particular, under moisture and thermal cycles [37]. However, existing works commonly concentrate on the unaged condition or the strain rate and temperature dependent property of adhesion [38, 39], other weathering actions such as damp heat, thermal cycles and radiation are not well studied.

The aim of this work is to investigate the effects of weathering actions on the bridging behaviour (bridging force, adhesion) between glass fragments with single EVA interlayer or hybrid EVA/PC interlayer. The hybrid interlayer is devised to provide better degradation resistance and

long-term post-fracture performance for LG products. First, both specimens for uniaxial tensile tests and TCT tests were exposed to weathering actions including different temperatures, damp heat, and radiations from laboratory light source. Uniaxial tensile tests were conducted to identify the stress strain relationship of the interlayers. TCT tests were subsequently performed on untreated and treated specimens to examine the local bridging behaviours near the crack. The testing data as well as the experimental observations such as delamination and rupture of interlayer were analysed to identify the effects of weathering actions on the local bridging effect of fractured glass laminates. Equivalent adhesion energy to describe the failure of interfacial bridging between fragments was also analysed, which adopted the simplified experimental theory of TCT tests and the data from uniaxial tensile tests.

2. Experimental study

2.1 Experimental theory of TCT tests

In a TCT test with ideal delamination state, i.e. the delamination front is parallel to the pre-defined cracks during progressive delamination, there is a coupling between delamination and the stretch of interlayer. As shown in Fig. 1 (a), once the TCT test reaches ideal delamination state, the load leading to progressive delamination is mainly sustained by the interlayer. In this stage, the interlayer has a total length of $2(\delta + a)$, where δ is the displacement of load head and a is the depth of the delaminated area (Fig. 1 (b)). The tensile stretch of the interlayer λ is given in Eq. (1):

$$\lambda = (\delta + a)/a = 1+\varepsilon_a \tag{1}$$

where ε_a is the steady state strain and can then be expressed as $\varepsilon_a = \delta/a$. As one significant property of adhesion, the total surface fracture energy per unit area of interlayer delamination, G_{tot}, can be calculated by introducing the energy balance approach [30]. It is assumed that the TCT system is without friction, hence, the external work done by the tensile force is equal to the sum of three components: (1) the strain energy stored in the interlayer, (2) energy dissipated to generate interlayer stretch, (3) the work used to increase the delamination depth a by an incremental growth da. The total surface fracture energy can be given as:

$$G_{tot} = (dW_{ext}/da - dW_s/da - dW_d/da)/b \tag{2}$$

where W_{ext} is the total external work injected into the TCT system, W_s denotes the energy stored in

the delaminated interlayer, W_d is the energy dissipated to generate the stretch of the delaminated interlayer. b is the specimen width.

The sum of dW_s and dW_d can be written as:

$$dW_s + dW_d = bh\mathrm{d}a \int_0^{\varepsilon_a} \sigma \mathrm{d}\varepsilon \tag{3}$$

where h is the interlayer thickness, σ is the tensile stress corresponding to the delamination force F. To calculate these two terms, the stress-strain relationships from the uniaxial tensile (UT) tests on the interlayer under each weathering action can be used. The total external work can be obtained through the TCT test:

$$dW_{ext} = F\, d\delta = F\, \mathrm{d}a\varepsilon_a \tag{4}$$

By substituting Eq.(3) and Eq.(4) into Eq.(2), the surface fracture energy G_a can be written as:

$$G_a = G_{tot}/4 = (\varepsilon_a F/b - h \int_0^{\varepsilon_a} \sigma \mathrm{d}\varepsilon)/4 \tag{5}$$

Note that there are four delaminated surfaces in a TCT specimen, thus, the fracture energy should be a quarter of the total surface fracture energy G_{tot}.

To describe the local bridging effect of fractured glass laminates under various weathering actions, it is significant to identify the associated influences on the following features: (1) the load-displacement behavior and the failure mode; (2) normalized force (F/b) and stress (F/bh); (3) Surface fracture energy of the glass-interlayer bonding surface. Therefore, both the UT tests and the TCT tests are required to be performed to obtain the above features.

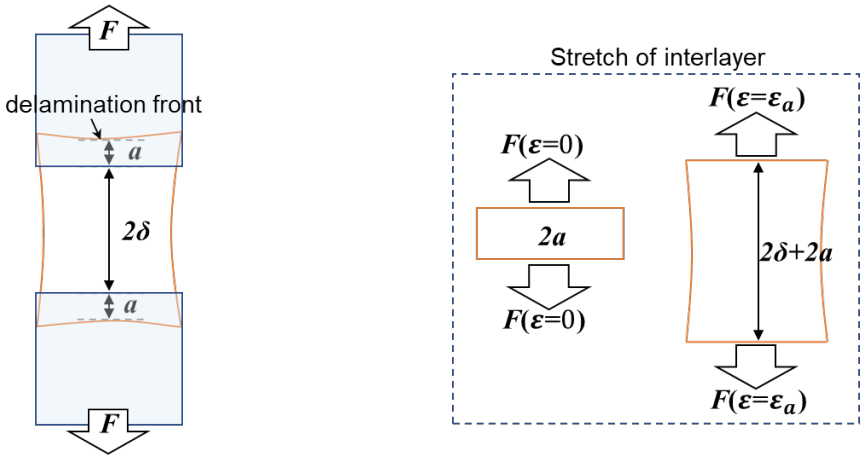

(a) TCT specimen under tension (b) Stretch of delaminated interlayer

Fig. 1 Schematic diagram of delamination and stretch of interlayer in TCT specimen

2.2 Artificial weathering treatment procedure

The specimens (both specimens for UT tests and TCT tests) were exposed to three types of artificial weathering actions including: 1) temperatures, 2) damp heat, 3) radiations from laboratory light source. For the action of temperatures, the temperatures were set from -20 °C to 100 °C at a 40 °C interval for the TCT specimens, whereas the temperatures were set from -20 °C to 120 °C at a 20 °C interval for the UT specimens to obtain finer results. The specimens were treated with the isothermal programme for more than one hour to ensure that it reached the desired temperature.

For the action of damp heat (DHT), a steady-state condition of 85 °C and 85% relative humidity (RH) was applied for at least 1000 hours. As for the radiation condition (RAD), Xenon-arc lamps were used to simulate the natural light source. The corresponding lighting procedure follows the Chinese standard GB/T 16422.2 [40] and is given in Table 1.

Table 1 Exposure cycles in the lighting procedure

Cycle No.	Exposure period	Irradiance		Black standard temperature (°C)	RH (%)
		Broadband (300 nm to 400 nm) (W/m^2)	Narrowband (340 nm) ($W/m^2 \cdot nm$)		
1	102 min dry 18 min water spray	60 ± 2	0.51 ± 0.02	65±3	50±10
2	102 min dry 18 min water spray	60 ± 2	0.51 ± 0.02	65±3	Not controlled
3	102 min dry 18 min water spray	60 ± 2	0.51 ± 0.02	100±3	20±10
4	102 min dry 18 min water spray	60 ± 2	0.51 ± 0.02	100±3	Not controlled

2.3 Tensile test on EVA based interlayers

The interlayer products, modified EVA interlayer (PVE®) and hybrid interlayer (SGE®), were provided by Shanghai HIUV New Materials Co., Ltd. The cross-link initiator of PVE material was peroxide. Several basic material performances of the interlayer products were given in Table 2. The PC material used to make SGE interlayer has a tensile modulus over 2200 MPa, a stress at break higher than 70 MPa. Its peak elongation can reach up to around 150% as given by the manufacturer. The dumb-bell shaped interlayer specimens were made according to the Chinese standard GB/T 528

[41], the dimensions of which are shown in Fig. 3 (a). The thickness of single polymer film, PVE and PC, was 0.38 mm before laminating to a thicker interlayer. For example, through laminating PVE layers to make thicker PVE products or stacking PVE and PC layers to make thicker SGE products, the nominal thickness of the PVE interlayer can be $0.38\times n_p$ (n_p = 1, 2, 3…), whilst that of SGE interlayer should be $0.38\times n_s$ (n_s = 3, 5, 7…). The nominal thicknesses of the PVE and the SGE interlayer for testing here were 1.52 mm (0.38 mm PVE × 4) and 1.14 mm (0.38 mm PVE/0.38 mm PC/0.38 mm PVE) (Fig. 3 (b)), respectively.

Table 2 Basic material performance of the EVA based interlayers

Type	Property	Range	Test method
Physical performance	Crosslinking Degree	≥85%	T/CPIA 0004 [42]
	180° Peeling strength	≥5N/mm (PVE) ≥10N/mm (SGE)	GB/T 2790 [43]
Optical performance	Light transmittance	≥86%	GB/T 2680 [44]
	Haze	≤0.7%	GB/T 2410 [45]

(a) PVE specimens after lighting procedure (b) PVE specimens after damp heat

Fig. 2 PVE specimens after damp heat and lighting treatment

The long weathering durations of damp heat and lighting procedure lead to the differences in the colour appearance of the specimens. It is seen that PVE material is more sensitive to the lighting action as the PVE specimens show more significant yellowing and present evident deformation (Fig. 2 (a)). Damp heat action does not yield such strong effect on the PVE material although the specimens are also found to show slight yellowing (Fig. 2 (b)). Similarly, the SGE specimens are seen to present slight yellowing without distinct deformation under both damp heat and lighting actions.

Followed by the weathering treatments, the tensile tests were carried out with a loading strain

rate of 0.2 s^{-1}. Five specimens of each interlayer were tested to ensure repeatability. The specimens under temperature treatment were directly tested in the isothermal chamber (Fig. 4 (a)). The other groups with damp heat and radiation treatment were firstly moved out of the weathering chambers and then tested immediately using the universal testing machine (Fig. 4 (b)).

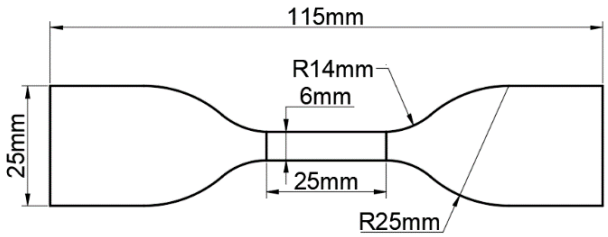

(a) Geometrical feature

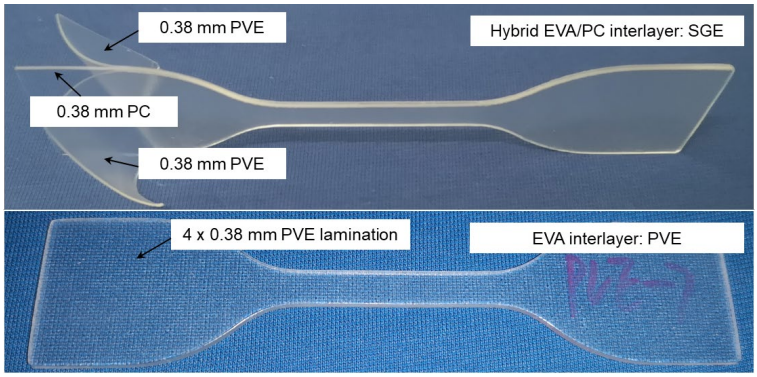

(b) Schematic of tested interlayer specimens

Fig. 3 Dimensions of the tensile tested specimens

(a) Isothermal chamber

(b) Extensometer and specimen

Fig. 4 Testing apparatus of UT tests on interlayers

The typical values of the stress-strain results were calculated and collected. The results of each interlayer under various temperatures are shown in Fig. 5. Fig. 5 (a) shows that the PVE interlayer

has excellent ductility before the temperature reaches 60 °C, where the failure strain is around 3.0. The failure strain will further decrease to nearly 1.2 with negligible tensile strength less than 1.0 MPa when temperature rises to 80 °C. The results from cases with higher temperature than 80 °C are not considered. When the temperature is lower than 60 °C, the stress-strain curves of the PVE material are of hyper-elastic nature, which commonly has a much lower tangent modulus with small strain and shows rapid increase when the strain is much larger. It can be seen that the PVE material presents an evident increase of tangent modulus when strain exceeds the value of around 3.0. It is also found that damp heat and radiation treatment facilitate the rupture of PVE material although the stress-strain relationship does not see evident difference when comparing with the test at 20 °C.

Fig. 5 (b) shows that the SGE interlayer presents a stress-strain relationship similar to elasto-plastic materials. It has a very high tangent modulus before the tensile strain reaches 0.1, which is followed by a short necking stage and later a plateau. The stress plateau ends from the strain of nearly 0.8 (-20 °C) to 1.34 (120 °C). Another short period of rising slope can also be found before the final failure. The results show that the SGE has performed satisfactorily in the high temperature range that covers the requirements of most of the practical designs.

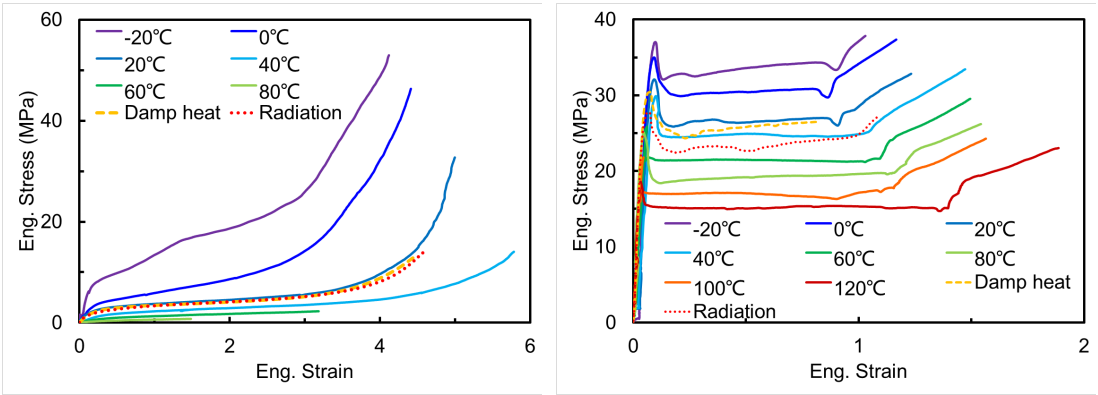

(a) PVE interlayer (b) SGE interlayer

Fig. 5 Typical stress-strain curves of specimens under various temperatures

The secant modulus within the strain interval (0-0.1) was then calculated, which can indicate the tensile stiffness of the interlayers. The elongation at failure and the failure stress of the PVE and SGE interlayer in each test were recorded and collected. Fig. 6 gives the collection of these three parameters under various temperatures. From Fig. 6 (a), the PVE interlayer has much lower modulus of up to 54 MPa at -20 °C and continuously decreases with the increase of temperature. The SGE

interlayer presents a smooth descending curve of secant modulus and has a minimum of greater than 150 MPa at 120 °C, showing an excellent stiffness capability under high temperature. Fig. 6 (b) shows that the SGE interlayer has very limited elongation at failure. The failure strain can only achieve a peak value of around 1.8, which is comparatively low amongst the polymeric interlayers in LG products. The elongation of the PVE interlayer grows from 400% at -20 °C up to nearly 540% at 40 °C. It can be seen in Fig. 6 (c) that the failure stress of the SGE interlayer varies from 39 MPa at -20 °C to 22.5 MPa at 120 °C, showing satisfactory tensile strength in high temperature. Although the PVE interlayer shows rapid degradation of tensile strength when temperature increases, its failure stress reaches more than 46 MPa at temperature lower than 0 °C, which is even higher than that of the SGE interlayer.

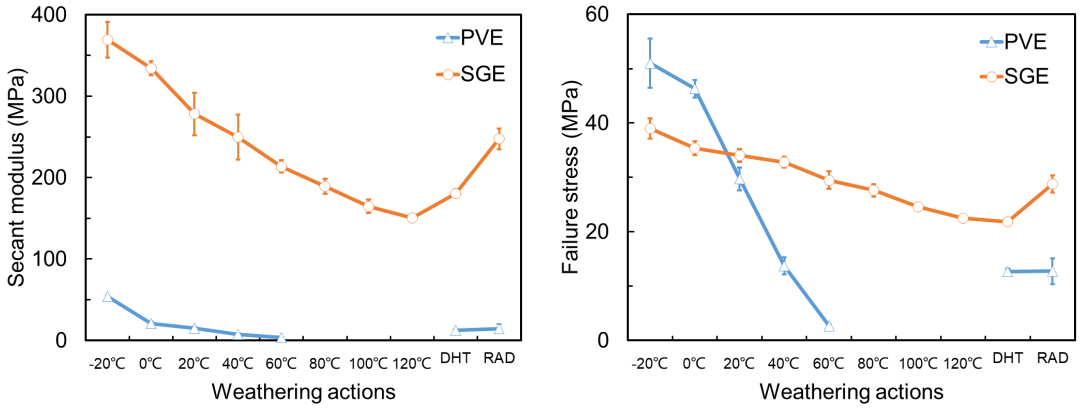

(a) Secant modulus (b) Elongation at failure

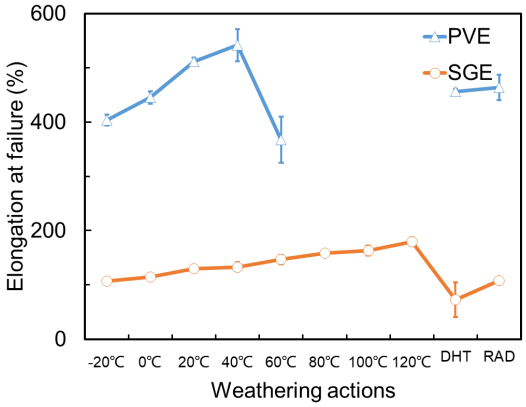

(c) Failure stress

Fig. 6 Secant modulus, elongation at failure and failure stress of PVE, SGE under various temperatures

2.4 Through-crack tensile test

Small TCT specimens (Fig. 7 (a)) were made by two steps: 1) lamination of annealed glass and interlayer, 2) trigger a through-crack at the centre of glass in both sides (Fig. 7 (a)). The lamination procedure is similar to that used for making LG products with PVB or SG interlayers, which includes rolling prelamination and autoclaving process. The temperature at the glass surface was set to be between 60-75°C for the PVE TCT specimens and 65-75°C for the SGE TCT specimens as suggested by the material supplier. The temperature in the autoclaving process was around 135-145°C and were kept stable for more than 60 mins (up to 90 mins). The dimensions of the specimens are designed to be 125 × 40 mm^2 and each glass layer has a nominal thickness of 5 mm. PVE interlayers having a nominal thickness of 0.76 mm (0.38 mm PVE × 2) were employed whilst double sheets of SGE interlayers with a nominal thickness of 2.28 mm (0.38 mm PVE/0.38 mm PC/0.76 mm PVE/0.38 mm PC/0.38 mm PVE) were used to make the TCT specimens. This is because the PVE TCT test is used to identify the interfacial property between glass and PVE, whereas the SGE TCT test aims to capture the potential progressive tearing or delamination which greatly affects the post-fracture behaviour of LG. In addition, it is also common to use thicker interlayers in China's market if stiffer interlayer type is required to be adopted. The actual thickness of the glass layers and the interlayer of each specimen after manufacturing were measured and recorded. The measured interlayer thickness of PVE varied from 0.60 mm to 0.69 mm. It is seen that the actual interlayer thicknesses of the PVE TCT specimens after the lamination process are rather scattered, which might be attributed to the fact that the used large autoclave is not able to guarantee adequate precision control of small size specimens using soft interlayers. The measured interlayer thicknesses of the SGE varied from 2.03 mm to 2.13 mm, showing higher consistency and slight reduction of the nominal thickness. This might be due to the laminated configuration of the EVA and PC layers could reduce the overflow of melting EVA materials and possibly introduce thickness loss.

Three TCT specimens of each weathering action were tested to ensure repeatability. Table 3 gives the list of the TCT specimens for weathering tests and their group IDs.

Table 3 List of TCT specimens for different weathering tests

ID	Interlayer type	Weathering action	Number
TEM_P1	PVE	-20°C	3

TEM_P2	PVE	20°C	3
TEM_P3	PVE	60°C	3
TEM_P4	PVE	100°C	3
DHT_P	PVE	damp heat	3
RAD_P	PVE	radiation	3
TEM_S1	SGE	-20°C	3
TEM_S2	SGE	20°C	3
TEM_S3	SGE	60°C	3
TEM_S4	SGE	100°C	3
DHT_S	SGE	damp heat	3
RAD_S	SGE	radiation	3

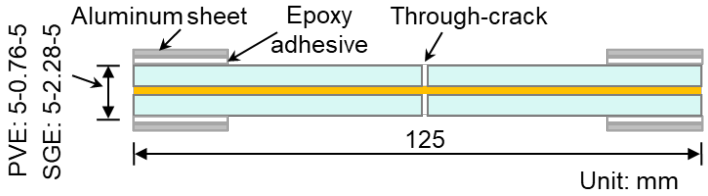

(a) Schematic of TCT specimen design

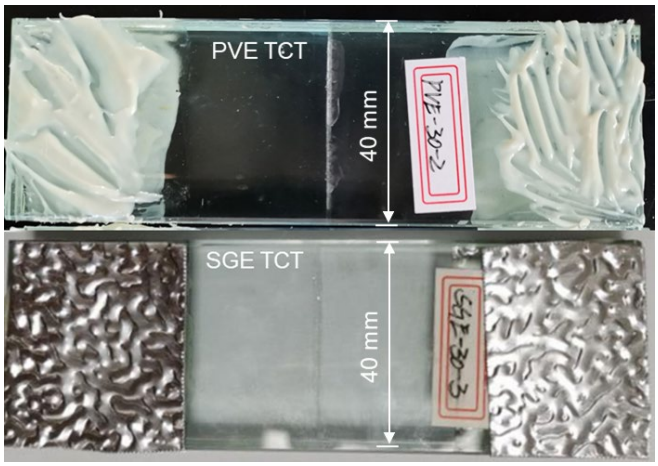

(b) Photo of tested specimen

Fig. 7 Design and photo of TCT specimen

Followed by the weathering treatment, the TCT specimens were subjected to uniaxial tensile load until failure occurred. In order to increase the friction of the smooth glass surface, epoxy adhesive (Silande MF1315) and thin aluminium sheets with rough surface were used at both ends of glass in the SGE TCT specimens. In the PVE TCT specimens, only epoxy adhesive was used at the glass surfaces (Fig. 7 (b)). TCT tests were performed on the specimens with a constant loading speed of 2 mm/s. The tensile force and displacement were recorded, and other properties such as progressive delamination and rupture of interlayer were closely monitored.

3. Results and discussion

3.1 Experimental observations

Based on the report by Elzière et al [46], the tensile behaviours of TCT specimens can be classified into three categories, i.e. unstable delamination, steady-state delamination and rupture. These categories also agree with the observations in our experiment. Fig. 8(a, b) shows the observed steady state delamination and unstable delamination behaviours of the PVE TCT tests, respectively. It can be seen that the delamination front is almost parallel to that of pre-defined cracks in the steady state delamination, whereas the delamination front is unstable and grows irregularly in the unstable delamination.

In the unstable delamination, the delamination propagates unevenly with undulated front. The uneven delamination leads to the growing difference in strain accumulation of interlayer, which is very likely to trigger interlayer rupture. Therefore, the development of unstable delamination can be frequently seen to end with the interlayer rupture.

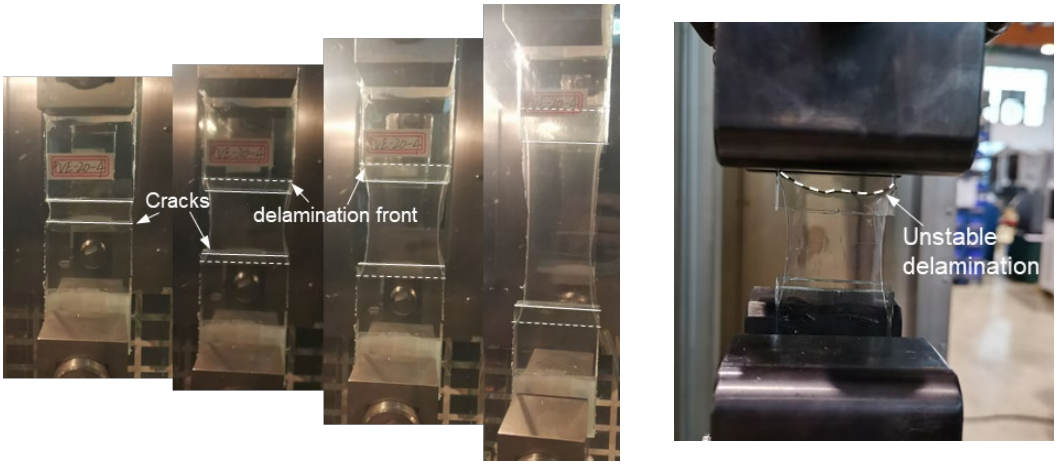

(a) Steady state delamination process (b) Unstable delamination

Fig. 8 Delamination behaviours observed in PVE TCT tests

3.2 Force-displacement relationships

Fig. 9 shows the force-displacement curves from the PVE TCT tests after weathering treatment. The corresponding category of tensile behaviors was assigned to the typical curves according to the experimental observations. From Figs. 9 (a2, c1), it can be seen that groups TEM_P2 and DHT_P

both present standard curves of steady state delamination, which can be characterized by a long and stable stage of force plateau after a force peak. The average force of the force plateau is defined as the steady state delamination force, which is found to be around 200 N in these two groups.

In group TEM_P1 (Fig. 9 (a1)), the consistency of the results amongst the same group is not ideal, showing that the PVE bonding surface has great sensitivity to low temperature. Despite this, in most TEM_P1 specimens, standard steady state delamination can still be found at the early stage of testing. Group TEM_P1 shows much higher delamination force than that of TEM_P2 (Fig. 9 (a2)), showing the enhancement of bonding strength due to low temperature. However, TEM_P1 enters the unstable delamination stage sooner and shows interlayer rupture at a displacement of 2-4 mm, which confirms that PVE materials become more brittle under a lower temperature.

From Figs. 9 (b1, b2), when temperature rises to 60 °C or higher, the delamination behaviour appears not the predominant factor of the local bridging behaviour near the through-cracks. It can be seen that the PVE interlayer has ruptured at a comparatively low tensile force, which varies from nearly 80 N to 100 N in TEM_P3 and declines to only 20 N in TEM_P4. Such a rupture force is much lower than the steady state delamination force in the other testing groups, for instance, nearly 200 N in TEM_P2 (Fig. 9 (a2)). Once the interlayer has ruptured, the tensile force suddenly drops to nearly zero, showing a complete loss of bridging effect. In other groups, the bridging effect gradually diminishes in a more ductile manner (e.g., see unstable delamination behaviour in TEM_P1), which is more favoured to post-fracture performance of glass laminates. Overall, the results show that high temperature (60 °C or higher) can result in brittle failure of the bridging parts between fragments, which will significantly damage the post-fracture capability.

From Fig. 9 (c2), only one specimen in RAD_P exhibits rupture during the unstable delamination. The other two specimens in RAD_P still present satisfactory steady state delamination with lower delamination force than that of group TEM_P2, showing the bonding surface of PVE to glass is still stable under the strong light sources. Note that the consistency of results in this group is not ideal which shows that the bonding surface is sensitive to the lighting condition.

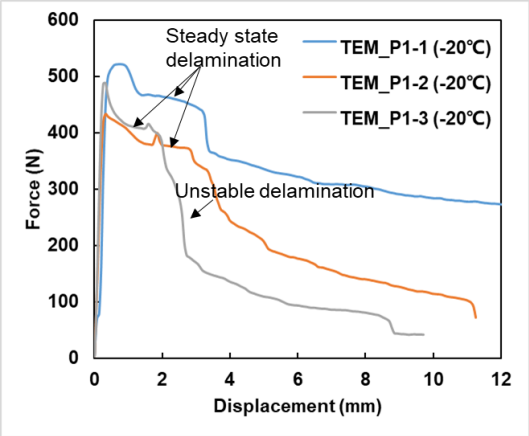

(a1) Thermal treatment (-20°C)

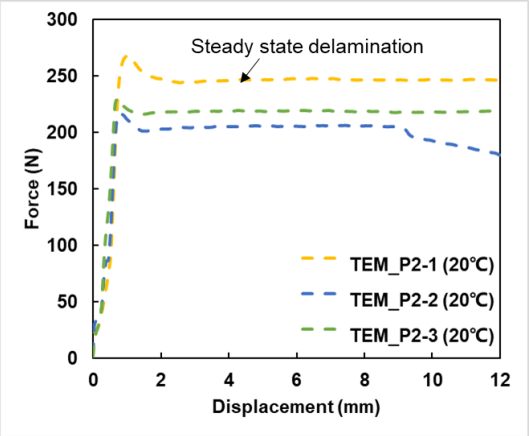

(a2) Thermal treatment (20°C)

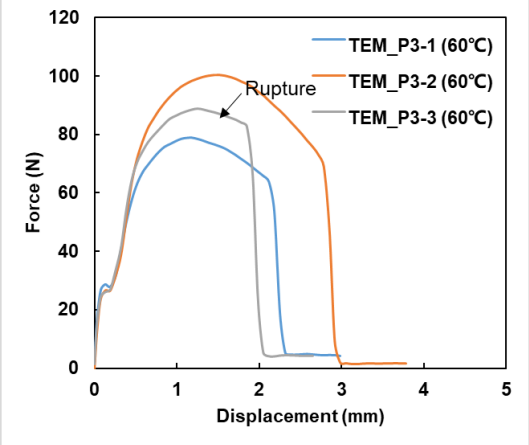

(b1) Thermal treatment (60°C)

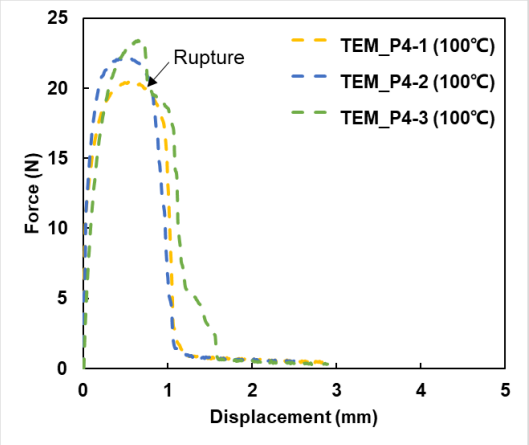

(b2) Thermal treatment (100°C)

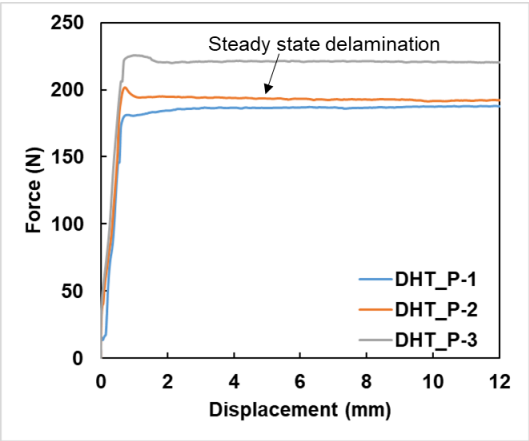

(c1) Damp heat treatment

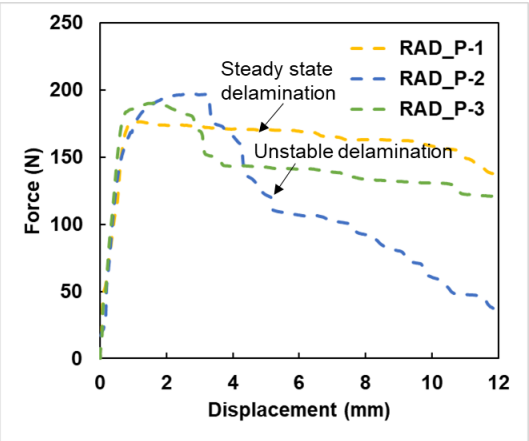

(c2) Radiation treatment

Fig. 9 Force-displacement results of PVE TCT tests

The traditional TCT tests were performed on the specimens laminated with single type of polymeric interlayer such as PVB interlayer. Thus, the tensile behaviour of the PVE TCT tests is expected to be similar to the experimental observations or trend of the testing data, which is

confirmed by the above experimental results. Differing from those with single type of polymeric interlayer, the results of the SGE TCT tests are expected to show multi-stage delamination or rupture as SGE is a composite interlayer that is expected to show internal delamination and rupture of different materials.

Fig. 10 gives the force-displacement curves of the SGE TCT tests. It can be clearly seen that most of the groups present multi-stage delamination or rupture behaviors except for group TEM_S4 (100 °C, see Fig. 10 (b2)), which has rapidly partial pulling out of middle composite layers (PC/PVE/PC) and subsequent unstable delamination. A typical force-displacement curve, e.g., from TEM_S2 (Fig. 10 (a2)) and RAD_S (Fig. 10 (c2)), is found to have two sudden drops which are due to the brittle rupture of the two PC layers. Fig. 11 shows the sequential rupture of the PC layers in group RAD_S.

Figs. 10 (a1, a2) shows the results of groups TEM_S1 (-20°C) and TEM_S2 (20°C). It is seen that both groups have two stages of steady state delamination. Although the tensile force of the steady state delamination stages in TEM_S1 exhibits slight oscillation, its overall trend is consistent. The steady state delamination forces of both the first and the second stages in TEM_S1 is higher than that in TEM_S2, whilst the corresponding increases are nearly 540 N in the first stage and 370 N in the second stage, respectively. The increases indicate that the SGE interlayer also has internal delamination at the PVE-PC surfaces in the first stage. To explain this, from Fig. 9 (a1, a2), the increase of steady state delamination force from TEM_P2 to TEM_P1 is nearly 170 N, which includes the contribution of the two Glass-PVE bonding surfaces. In TEM_S1 and TEM_S2, in addition to the two Glass-PVE bonding surfaces, there are four PVE-PC surfaces that can resist the delamination force. In the second stage of steady state delamination, one PC layer tears and thus only two Glass-PVE surfaces and two PVE-PC surfaces are intact and provide a force increase of 370 N in TEM_S1. It is then easy to find that the two Glass-PVE surfaces can contribute an increase of nearly 170 N delamination force whilst the two PVE-PC surfaces can contribute an increase of 200 N when temperature varies from 20°C to -20°C. It is then inferred that the increase of 540 N in the first steady state delamination stage of TEM_S1 encompasses the force to facilitate the internal delamination of the SGE interlayer.

In Fig. 10 (b1), the results from group TEM_S3 under thermal treatment of 60 °C show consistent trend, which is characterized by steady state delamination, subsequent rupture of PC

layers and unstable delamination in sequence. The steady state delamination force of TEM_S3 is around 2000 N, which is nearly 30% lower than that of TEM_S2 (20 °C) (Fig. 10 (a2)), indicating a significant degradation of bonding due to the temperature rise. This becomes worse when temperature goes up to 100 °C (Fig. 10 (b2)), at which the internal composite layers (PC/PVE/PC) are pulled out in a sudden when tensile force reaches nearly 1500 N. The specimens subsequently enter unstable delamination stage with very limited resistance.

Most specimens under damp heat (Fig. 10 (c2)) can exhibit clear stages of steady state delamination and rupture of PC layers, except for DHT_S-3 of which the composite SGE interlayer tears gradually and hence does not show steady state delamination. This might be caused by the unappropriated edge finishing of specimen which leads to flaws at the edges of SGE interlayer and further triggers the early rupture. It is also found that the steady state delamination forces in groups DHT_S and RAD_S are very close, which indicates that the influence caused by damp heat and radiation actions on the adhesion resistance is limited. However, it is seen that specimens under damp heat present a trend of facilitating interlayer rupture whereas the interlayers in those under radiation action are less likely to tear under small displacement.

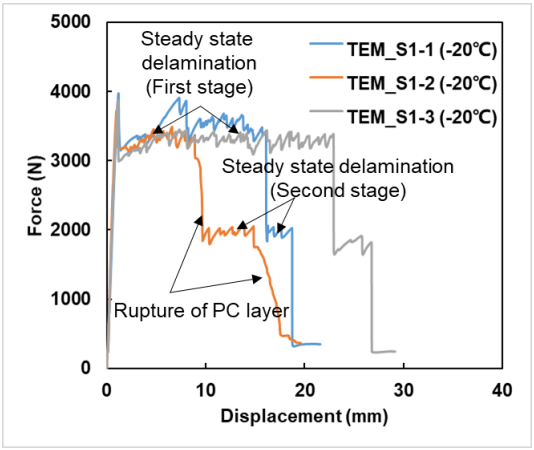

(a1) Thermal treatment (-20°C)

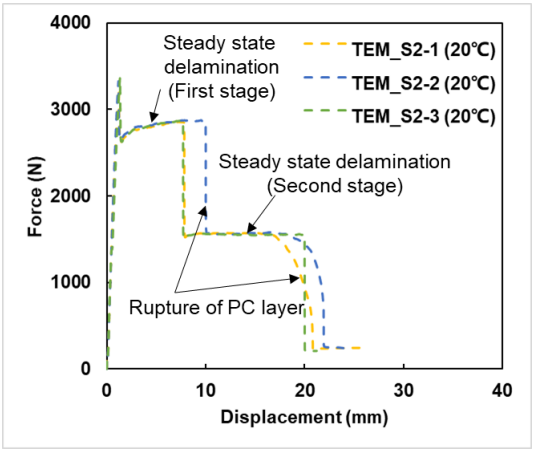

(a2) Thermal treatment (20°C)

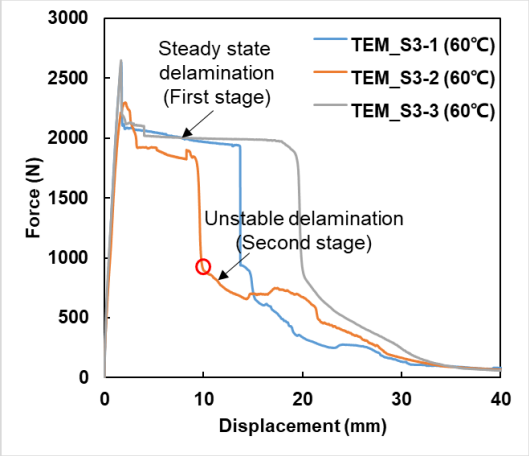

(b1) Thermal treatment (60°C)

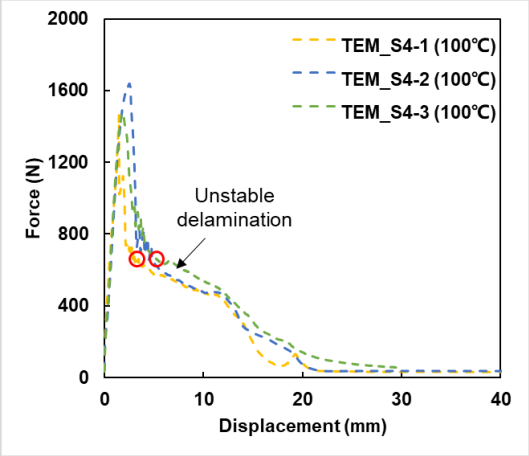

(b2) Thermal treatment (100°C)

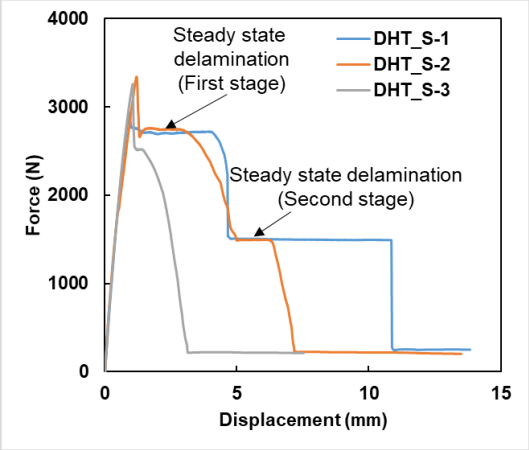

(c1) Damp heat treatment

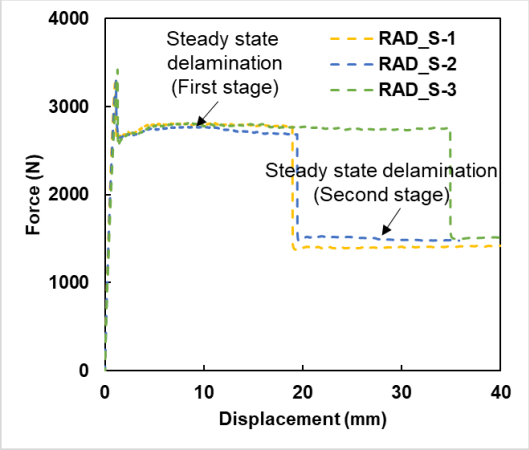

(c2) Radiation treatment

Fig. 10 Force-displacement results of SGE TCT tests

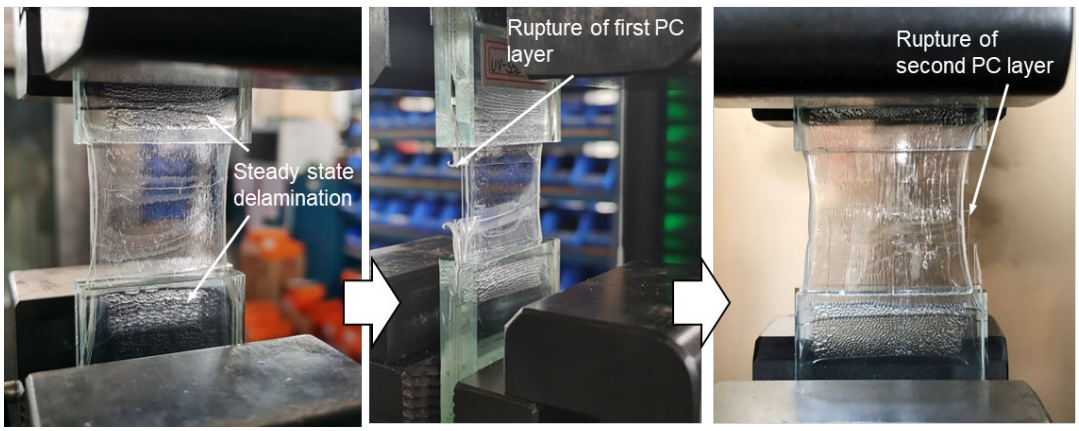

Fig. 11 Progressive delamination and rupture in SGE TCT specimens

3.3 Normalized force and stress

In Fourton's work [29], the normalized force, which is named as adherence energy and is defined as the tensile force F divided by the sample width b, was used to identify the transition between different TCT categories. The transition was found to be related to both tensile velocity and temperature. The concept of the normalized force was adopted here to present the difference of the bridging adherence energy in the PVE and SGE TCT specimens under various weathering actions. The normalized stress which is defined as F divided by b and actual interlayer thickness h, was also employed as it indicates the nominal failure stress of the bridged glass fragments.

In the PVE TCT tests, the tensile force F was defined as the steady state delamination force (TEM_P1, TEM_P2, DHT_P, RAD_P) or the peak rupture force in TEM_P3 and TEM_P4 groups. The collected mean values and standard deviations of the normalized force (F/b) and the normalized stress (F/bh) in each group of the PVE TCT tests can be found in Fig. 12. The high sensitivity of the PVE material to the temperature can be clearly seen, which leads to a consistent decline of the normalized force and stress with the increase of the temperature. With very low temperature of -20 °C, the normalized force and stress are significantly scattered, which shows the nonuniformity of bonding enhancement due to the low temperature. In TEM_P2, the normalized force has a mean value of 5.5 N/mm at a loading displacement rate of 2 mm/s. This value is slightly lower than the reported normalized force (nearly 6 N/mm) of PVB TCT at a loading displacement rate of 1 mm/s and same loading temperature in refs [29, 46]. Considering that a higher loading displacement rate will generate higher normalized force as indicated by the existing works, it implies that the adherence energy of the PVE-glass surface is lower than that of the PVB-glass surface at ambient temperature.

The effects of damp heat and radiation on the normalized force of PVE TCT are relatively lower when comparing with those of high temperature. The mean normalized forces of DHT_P and RAD_P are, respectively, 10.9% and 21.8% lower than that of TEM_P2. However, when the actual interlayer thickness is used, the normalized stress of DHT_P and RAD_P are further reduced by 29.6% and 37.0%, respectively. In fact, the normalized stress refers to the tensile strength at the through-cracks before delamination occurs, which encompasses the contribution of the interlayer. The decrease in the normalized stress is higher that the decrease in the normalized force, which

indicates that the damp heat has greater effects on the interlayer property than the interfacial property. Analogously, it can be concluded that the radiation action can result in a higher degradation of interfacial property than interlayer property. This can also be supported from the force-displacement curves of RAD_P in Fig. 9(c), which shows that the glass-PVE interface is more likely to have unstable delamination after a short period of steady state delamination when subjected to the radiation action, whereas the interface in DHT_P is more stable with consistent steady state delamination.

More than 90% of the normalized force and stress in TEM_P2 are lost when temperature rises to 100°C in TEM_P4, showing that bridging capability between PVE-glass fragments is very limited.

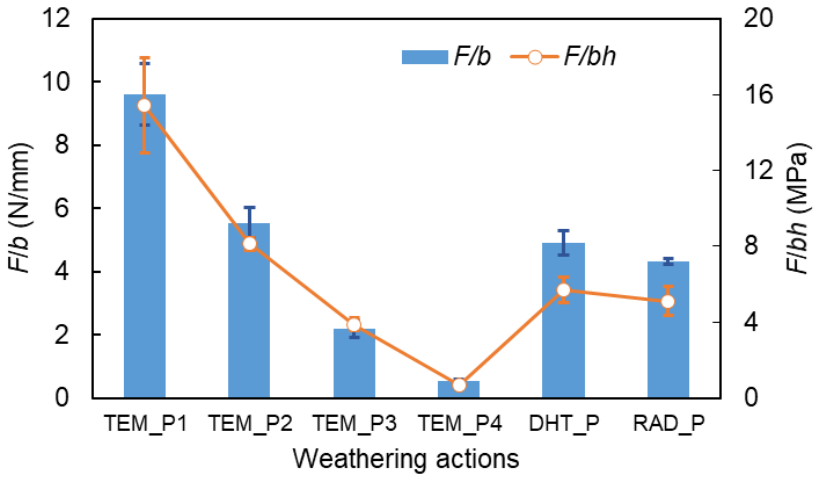

Fig. 12 Normalized force and stress results of PVE TCT tests

In the SGE TCT tests, two types of tensile force F were defined for the multi-stage delamination. In the first stage, F was defined as the steady state delamination force (TEM_S1, TEM_S2, TEM_S3, DHT_S, RAD_S) or the peak delamination force in TEM_S4. In the second stage, F was determined as the steady state delamination force (TEM_S1, TEM_S2, DHT_S, RAD_S) or the value at the transition from the sudden force drop and progressively unstable delamination (TEM_S3, TEM_S4, see red circles as example in Fig. 10 (b)). The normalized force and stress in the different stages of SGE TCT tests are given in Fig. 13(a), (b), respectively.

It can be seen that for the polycarbonate layer(s), the normalized force and stress from the SGE TCT tests are significantly higher than those from the PVE TCT tests. The TEM_S4 group is also found to remain a high capability of connecting glass fragments under 100°C treatment, in which

the normalized force and stress in the first stage (Fig. 13(a)) are 37.7 N/mm, 17.7 MPa, respectively. In the second stage, TEM_S4 presents progressively unstable delamination and its transition values of the normalized force and stress are 18.5 N/mm and 8.7 MPa, respectively (Fig. 13(b)). In contrast, TEM_P4 with one PVE layer lost most of such capability. Besides, the degradation trend of the results from other weathering actions is similar to that of the PVE TCT tests, which can be characterized with two main trends. First, the normalized force and stress keep declining when temperature rises from -20°C to 100°C. Second, the damp heat and radiation treatment can cause the values of normalized force and stress between those under 20°C and 60°C, although the decrease of results under damp heat and radiation treatment from those under 20°C is much less significant in SGE.

An interesting finding is that the normalized stress of the SGE TCT specimens in the first stage is very close to the yield stress at the end of elastic stage of the SGE interlayer in Fig. 5 (b). This indicates that the bridging mechanism of the adopted configuration of SGE can efficiently utilise both the interfacial bonding strength and the interlayer strength, which presents an ideal bridging failure mode.

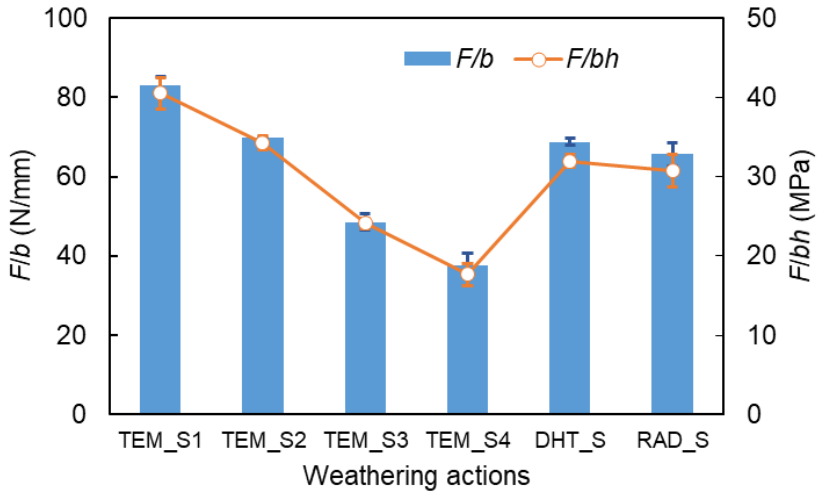

(a) First stage

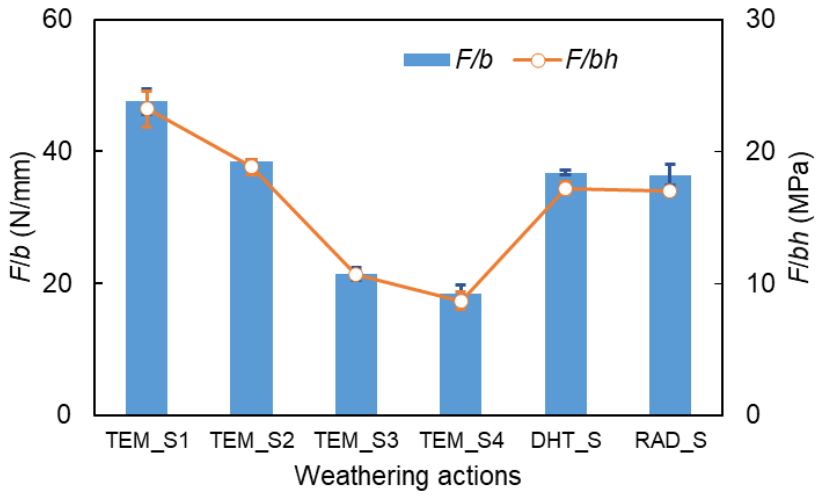

(a) Second stage

Fig. 13 Normalized force and stress results of SGE TCT tests

Trends of normalized force and stress similar to the first stage can also be seen in the second stage of the SGE TCT tests. The average ratios of decrease of the normalized force and stress in the second stage when comparing with those in first stage under diverse weathering actions were collected and shown in Fig. 14. It is seen that the ratios for both normalized force and stress are very close in each weathering action. For groups with steady state delamination, i.e. TEM_S1/S2, DHT_S and RAD_S, the ratio of decrease varies from 42.7% to 46.5%. In the other groups, the ratio increases to 50.9% in TEM_S4 and 55.8% in TEM_S3, respectively.

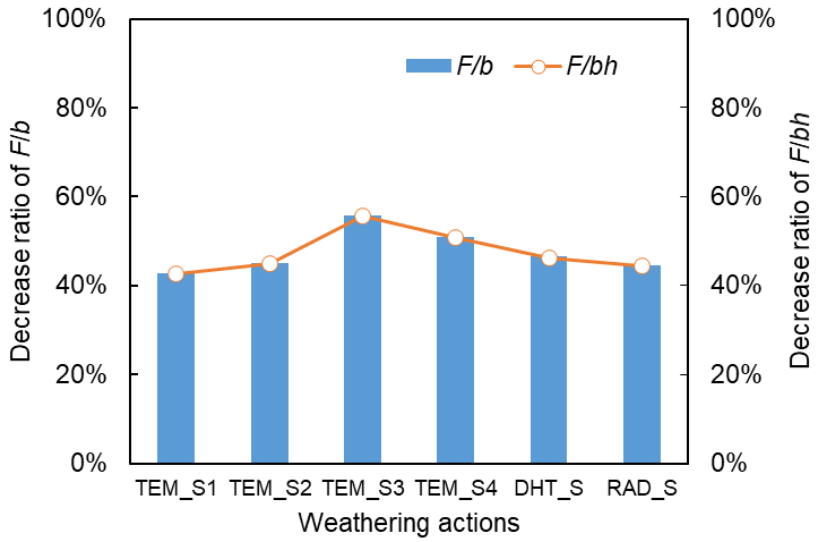

Fig. 14 Decrease ratio of normalized force and stress in second stage from SGE TCT tests

3.4 Equivalent adhesion energy

As described in Section 2.1, TCT tests can be used to identify the surface fracture energy of the glass-interlayer bonding surface if ideal delamination state is seen, i.e. in a steady state delamination state. However, the weathering action significantly affects the delamination progress of PVE and SGE specimens, in particular, in high temperature. Furthermore, the experimental theory was originally developed for single type of interlayer without considering the interlaminar delamination of composite interlayers. As the unstable delamination or the interlamination of composite interlayer also indicates the capability to resist the failure of bridging effects between glass fragments, in this section, it is assumed that the contribution of interlaminar delamination of composite interlayers as well as the unstable delamination is reflected in the presence of total adhesion energy and peak tensile force. Therefore, for those cases without steady state delamination state (TEM_P3, TEM_P4 and TEM_S4), the adhesion energy will be calculated using peak tensile force instead of steady state delamination force. For the SGE TCT specimens having steady state delamination state, the adhesion energy will still be calculated using steady state delamination force to obtain an equivalent value (pseudo value). The corresponding surface fracture energy is seen as equivalent delamination energy.

Mean values and standard deviations of the equivalent delamination energies calculated from the PVE and SGE TCT tests are shown in Fig. 15. The results of the SGE TCT tests include those from both the first and the second stage. In most weathering actions, the adhesion energy of the PVE specimens, of which the peak mean value is 467 J/m^2 at 20°C, is higher than that of the SGE specimens in the second stage. As for the SGE specimens in the first stage, because of the contribution of interlaminar delamination to the total work of delamination, the equivalent adhesion energy increases more significantly than for the PVE specimens except for high temperature cases. The adhesion energy of the SGE specimens in the first stage is found to has a peak value of 1112 J/m^2 at -20°C and decrease to around 984 J/m^2 at 20°C. It also confirms several conclusions drawn in the above sections, for example, damp heat and radiation can damage the adhesion ability of SGE to glass, as the adhesion energy is seen to decline to around 600 J/m^2 and 400 J/m^2, respectively.

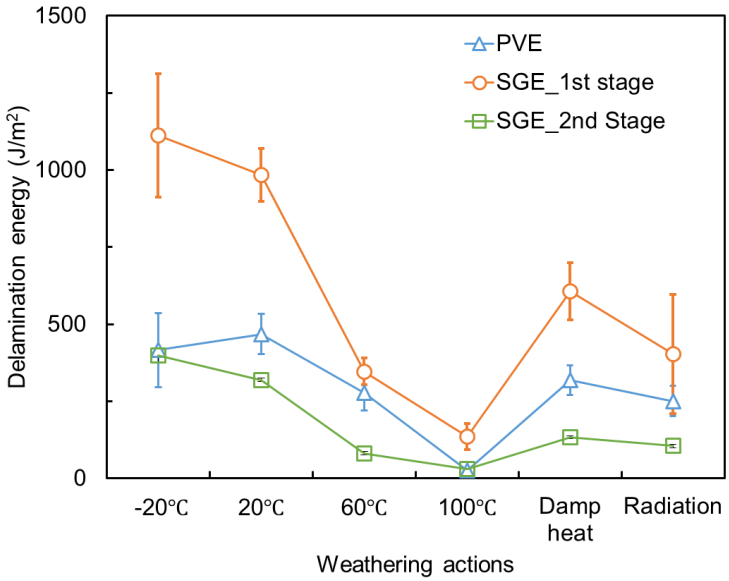

Fig. 15 Equivalent adhesion energy from PVE and SGE TCT tests

4. Conclusions

This work has investigated the bridging effects between fractured glass laminates having EVA based interlayers and subjected to various weathering treatments, such as temperature, damp heat and lighting treatment. Both single EVA interlayer (PVE) and hybrid EVA/PC interlayer (SGE) were considered. Through-crack tensile tests were performed on the treated specimens to examine the bridging effects, whilst the uniaxial tensile tests on treated interlayers were also carried out to identify the degradation of adhesion properties. Several key findings were summarized and shown below:

(1) Three categories of tensile behaviors in the through-crack tensile tests on fractured glass laminates with EVA based interlayers were observed, which were steady-state delamination, unstable delamination and rupture. The latter two categories were frequently seen when temperature rises to over 60℃.

(2) The high sensitivity of PVE to low temperature will lead to the enhancement of adhesion strength and greater brittleness of PVE material. The strong lighting treatment is found to damage the adhesion ability of PVE to glass, although the adhesion surface is still comparatively stable. High temperature (60 °C or higher) is the dominant factor which can result in brittle failure of the bridging effects between glass fragments. The resistance to the bridging failure is very limited when

temperature rises to 100°C both with PVE and SGE interlayers.

(3) The bridging failure of SGE laminated glass is characterized by multi-stage delamination or ruptures of polymeric layers. High temperature treatment (100°C) will result in rapid loss of bridging ability. The residual resistance to bridging failure after the first stage of delamination or rupture is found to have a trough value of nearly 44% and a peak of nearly 58% of the original resistance.

(4) Damp heat and lighting treatment have limited effects on the adhesion properties of SGE. However, the former is seen to facilitate interlayer rupture and the latter is less likely to trigger early stage tearing of interlayer. The radiation will also decrease adhesion energy more than damp heat will.

Data availability

The data that supports the findings of this study are available within the article.

CRediT authorship contribution statement

Jian Yang: Writing – Original Draft, Investigation, Funding acquisition. **Yige Wang**: Investigation, Formal analysis. **Xing-er Wang**: Writing – Original Draft, Supervision, Funding acquisition. **Xiaonan Hou**: Writing -Review & Editing, Validation. **Chenjun Zhao**: Data curation, Visualization. **Jianqiao Ye**: Writing -Review & Editing.

Declaration of Competing Interest

The authors declare that they have no known competing financial interests or personal relationships that could have appeared to influence the work reported in this paper.

Acknowledgement

This study was funded by the National Natural Science Foundation of China [Grant No. 52078293,51908352] and the Shanghai Science and Technology Innovation Action Plan [Grant No. 20dz1201301].

References

[1] Zhang X, Liu H, Maharaj C, Zheng M, Mohagheghian I, Zhang G, et al. Impact response of laminated glass with varying interlayer materials. International Journal of Impact Engineering. 2020;139:103505.

[2] Hooper PA, Sukhram RAM, Blackman BRK, Dear JP. On the blast resistance of laminated glass. International Journal of Solids and Structures. 2012;49(6):899-918.

[3] Wang X-E, Meng Y, Yang J, Huang X, Wang F, Xu H. Optimal kernel extreme learning machine model for predicting the fracture state and impact response of laminated glass panels. Thin-Walled Structures. 2021;162:107541.

[4] Wang X-E, Yang J, Chong WTA, Qiao P, Peng S, Huang X. Post-fracture performance of laminated glass panels under consecutive hard body impacts. Composite Structures. 2020;254:112777.

[5] D'Ambrosio G, Galuppi L, Royer-Carfagni G. A simple model for the post-breakage response of laminated glass under in-plane loading. Composite Structures. 2019;230:111426.

[6] Saputra A, Behnke R, Xing W, Song C, Schneider J, Kaliske M. Numerical representation of fracture patterns and post-fracture load-bearing performance of thermally prestressed glass with polymer foil. Engineering Structures. 2021;226:111318.

[7] Biolzi L, Orlando M, Piscitelli LR, Spinelli P. Static and dynamic response of progressively damaged ionoplast laminated glass beams. Composite Structures. 2016;157:337-47.

[8] Biolzi L, Cattaneo S, Orlando M, Piscitelli LR, Spinelli P. Post-failure behavior of laminated glass beams using different interlayers. Composite Structures. 2018;202:578-89.

[9] Galuppi L, Royer-Carfagni G. The post-breakage response of laminated heat-treated glass under in plane and out of plane loading. Composites Part B: Engineering. 2018;147:227-39.

[10] D'Ambrosio G, Galuppi L, Royer-Carfagni G. Post-breakage in-plane stiffness of laminated glass: an engineering approach. Glass Structures & Engineering. 2019;4(3):421-32.

[11] Galuppi L, Royer-Carfagni G. A homogenized model for the post-breakage tensile behavior of laminated glass. Composite Structures. 2016;154:600-15.

[12] Zhao C, Yang J, Wang X-e, Azim I. Experimental investigation into the post-breakage performance of pre-cracked laminated glass plates. Construction and Building Materials. 2019;224:996-1006.

[13] Wang X-E, Yang J, Pan Z, Wang F, Meng Y, Zhu Y. Exploratory investigation into the post-fracture model of laminated tempered glass using combined Voronoi-FDEM approach. International Journal of Mechanical Sciences. 2020:105989.

[14] Wang X-E, Yang J, Huang X, Wang F, Zhu Y. Voronoi-FDEM concept for modelling post-fracture response of progressively damaged structural glass. Engineering with Computers. 2021.

[15] Wang X-E, Yang J, Liu Q, Zhao C. Experimental investigations into SGP laminated glass under low velocity impact. International Journal of Impact Engineering. 2018;122:91-108.

[16] Martín M, Centelles X, Solé A, Barreneche C, Fernández AI, Cabeza LF. Polymeric interlayer materials for laminated glass: A review. Construction and Building Materials. 2020;230:116897.

[17] Hána T, Vokáč M, Eliášová M, V. Machalická K. Experimental investigation of temperature and loading rate effects on the initial shear stiffness of polymeric interlayers. Engineering Structures. 2020;223:110728.

[18] Chen S, Chen X, Wu X. The mechanical behaviour of polyvinyl butyral at intermediate strain rates and different temperatures. Construction and Building Materials. 2018;182:66-79.

[19] Biolzi L, Cattaneo S, Orlando M, Piscitelli LR, Spinelli P. Constitutive relationships of different

interlayer materials for laminated glass. Composite Structures. 2020;244:112221.
[20] Centelles X, Castro JR, Cabeza LF. Experimental results of mechanical, adhesive, and laminated connections for laminated glass elements – A review. Engineering Structures. 2019;180:192-204.
[21] Nawar M, Salim H, Newberry M, El-Sisi A. High strain rate response of laminated glass interlayer materials. Construction and Building Materials. 2021;299:123934.
[22] Chen S, Lu Y, Zhang Y, Shao X. Experimental and analytical study on uniaxial tensile property of ionomer interlayer at different temperatures and strain rates. Construction and Building Materials. 2020;262:120058.
[23] Centelles X, Martín M, Solé A, Castro JR, Cabeza LF. Tensile test on interlayer materials for laminated glass under diverse ageing conditions and strain rates. Construction and Building Materials. 2020;243:118230.
[24] Schuster M, Kraus M, Schneider J, Siebert G. Investigations on the thermorheologically complex material behaviour of the laminated safety glass interlayer ethylene-vinyl-acetate. Glass Structures & Engineering. 2018;3(2):373-88.
[25] Hänig J, Weller B. Load-bearing behaviour of innovative lightweight glass–plastic-composite panels. Glass Structures & Engineering. 2020;5(1):83-97.
[26] Zhang B, Guo X, Liu Y, Lang L, Tan S. Study of glass laminate configurations on ballistic resistance of novel lightweight sapphire transparent laminated structures. International Journal of Lightweight Materials and Manufacture. 2021;4(4):397-404.
[27] Delincé D. Experimental approaches for assessing time and temperature dependent performances of fractured laminated safety glass. Ghent: Ghent University; 2014.
[28] Seshadri M, Bennison SJ, Jagota A, Saigal S. Mechanical response of cracked laminated plates. Acta Materialia. 2002;50(18):4477-90.
[29] Fourton P, Piroird K, Ciccotti M, Barthel E. Adhesion rupture in laminated glass: influence of adhesion on the energy dissipation mechanisms. Glass Structures & Engineering. 2020;5(3):397-410.
[30] Samieian MA, Cormie D, Smith D, Wholey W, Blackman BRK, Dear JP, et al. On the bonding between glass and PVB in laminated glass. Engineering Fracture Mechanics. 2019;214:504-19.
[31] Nhamoinesu S, Overend M, editors. Simple models for predicting the post-fracture behaviour of laminated glass. In the Proceedings of the XXV ATIV 2010, International Conference, Parma, Italy; 2010.
[32] Froli M., Lani L. Adhesion, creep and relaxation properties of pvb in laminated safety glass. Glass Performing Days; Tampere, Finland, 2011. p. 1-4.
[33] Schneider K, Lauke B, Beckert W. Compression Shear Test (CST) – A Convenient Apparatus for the Estimation of Apparent Shear Strength of Composite Materials. Applied Composite Materials. 2001;8(1):43-62.
[34] Schuster M, Schneider J, Nguyen TA. Investigations on the execution and evaluation of the Pummel test for polyvinyl butyral based interlayers. Glass Structures & Engineering. 2020;5(3):371-96.
[35] Rahul-Kumar P, Jagota A, Bennison SJ, Saigal S. Interfacial failures in a compressive shear strength test of glass/polymer laminates. International Journal of Solids and Structures. 2000;37(48):7281-305.
[36] Centelles X, Castro JR, Cabeza LF. Double-lap shear test on laminated glass specimens under diverse ageing conditions. Construction and Building Materials. 2020;249:118784.
[37] Rivers G, Cronin D. Influence of moisture and thermal cycling on delamination flaws in transparent

armor materials: Thermoplastic polyurethane bonded glass-polycarbonate laminates. Materials & Design. 2019;182:108026.
[38] Bermbach T, Teich M, Gebbeken N. Experimental investigation of energy dissipation mechanisms in laminated safety glass for combined blast-temperature loading scenarios. Glass Structures & Engineering. 2016;1(1):331-50.
[39] Angelides SC, Talbot JP, Overend M. High strain-rate effects from blast loads on laminated glass: An experimental investigation of the post-fracture bending moment capacity based on time–temperature mapping of interlayer yield stress. Construction and Building Materials. 2021;273:121658.
[40] Standardization Administration of China. GB/T 16422.2 Plastics - Methods of exposure to laboratory light sources - Part 2: Xenon-arc sources. Beijing: Standards Press of China; 2014.
[41] Standardization Administration of China. GB/T 528 Rubber, vulcanized or thermoplastic - Determination of tensile stress-strain properties. Beijing: Standards Press of China; 2009.
[42] China photovoltaic industry association. T/CPIA 0004 Ethylene-vinyl acetate copolymer (EVA) film for photovoltaic module. Beijing, 2017.
[43] Ministry of Chemical Industry of the PRC. GB/T 2790 Adhesives, 180° peel strength test method for a flexible-bonded-to-rigid test specimen assembly. Beijing: The State Bureau of Quality and Technical Supervision; 1995.
[44] State Administration for Market Regulation. GB/T 2680 Glass in building-Determination of light transmittance, solar direct transmittance, total solar energy transmittance, ultraviolet transmittance and related glazing factors. Beijing: Standardization adminstration; 2021.
[45] General Administration of Quality Supervision Inspection and Quarantine of the PRC. GB/T 2410 Determination of the luminous transmittance and haze of transparent plastics. Beijing: Standardization adminstration; 2008.
[46] Elzière P, Dalle-Ferrier C, Creton C, Barthel É, Ciccotti M. Large strain viscoelastic dissipation during interfacial rupture in laminated glass. Soft Matter. 2017;13(8):1624-33.